APPLYING MPSO FOR BUILDING SHEAR WAVE VELOCITY MODELS FROM MICROTREMOR RAYLEIGH-WAVE DISPERSION CURVES

A. ZAREAN[1], N. MIRZAEI[2] and M. MIRZAEI[3]

[1] *Department of Geophysics, Science and Research Branch, Islamic Azad University, P.O. Box 14778-93855, Tehran, Iran. a.zarean@iaushab.ac.ir*
[2] *Institute of Geophysics, University of Tehran, P.O. Box 14155-6466, Tehran, Iran.*
[3] *Department of Physics, University of Arak, Arak, Iran.*

(Received August 24, 2014; revised version accepted December 3, 2014)

ABSTRACT

Zarean, A., Mirzaei, N. and Mirzaei, M., 2015. Applying MPSO for building shear wave velocity models from microtremor Rayleigh-wave dispersion curves. *Journal of Seismic Exploration*, 24: 51-82.

Surface waves have been increasingly used as an attractive tool for obtaining near-surface shear-wave velocity profiles. Inversion of surface wave dispersion curves is a challenging problem for most of local-search methods due to their high nonlinearity and multimodality (large numbers of local minima and maxima of the misfit function). Rayleigh- and Love-wave dispersion curves derived from microtremor arrays have the advantage of not requiring artificial sources; however, they have disadvantages of high uncertainty, low sampling number and limited frequency band. Among many approaches which have been proposed for surface wave inversion thus far, metaheuristic algorithms have been effectively applied to solve it, and avoid trapping in local minima. In this study, a hybrid approach was proposed for inversion of surface wave dispersion curves. The method is a genetic algorithm mutation based particle swarm optimization, namely MPSO. The mention for using the additional mutation operator in this study was to prevent early convergence on local optima of the solution. In each iteration, a hybrid mutation scheme was applied to search the neighborhood area of the solution which corresponds to the two best particles: the best current particle and the best particle found so far. The population was divided into two parts; the first one was regenerated according to the particle swarm optimization and the latter was generated by applying the proposed here. In this work, in order to invert the dispersion curves, a new MATLAB code was developed for the MPSO algorithm. Also, to evaluate calculation efficiency and MPSO stability for inversion of surface wave data, various synthetic dispersion curves were inverted. Following this stage, a comparative analysis with the original particle swarm optimization and the genetic algorithm was made. Consequently, using the MPSO algorithm, the Rayleigh-wave dispersion curve was inverted and one-dimensional V_S profiles were obtained. In conclusion, the proposed approach represents an improvement of a purely particle swarm optimization scheme and the MPSO typically offers a more significant and precise solution in the case of synthetic models. Results of inversion performed on a field data set were validated by borehole stratigraphy.

KEY WORDS: particle swarm optimization, mutation, Rayleigh-wave, dispersion curves, microtremor.

0963-0651/15/$5.00

INTRODUCTION

Shear-wave velocity (V_S) is an important parameter for site characterization in geotechnical engineering (Renalear et al., 2010). In theory, V_S is a function of ground compactness and rigidity variations (Hunter et al., 2002). Also, V_S imaging techniques allow for delineation of geologic boundaries in the subsurface. In earthquake engineering, ground motion characteristics including amplitude and duration are amplified in sites where soft soil layers cover firm bedrock. This is in contrast to V_S values that strongly control dynamic site response and the resulting damage (Bard and Riepl, 1999; Somerville and Graves, 2003). So, V_S is required for evaluating site effects in seismic hazard assessment. Shear-wave velocity (V_S) is in situ measured by various methods including borehole tests, shear-wave refraction and reflection studies and surface-wave techniques (Jongmans, 1992; Dasios et al., 1999; Hunter et al., 2002; Boore, 2006). In recent years, surface waves have been increasingly used for deriving V_S as a function of depth (e.g., Socco and Jongmans, 2004).

The applied surface-wave method shares the same procedure to other surface-wave analysis methods, which also can be concluded by these three main steps (Socco et al., 2010):

1. Acquire the experimental data.
2. Process the signal to obtain the experimental dispersion curve.
3. Solve the inverse problem to estimate model parameters.

Each step can be performed using different approaches according to the scale of the problem, target, complexity of the subsoil property distribution and available equipment and budgets. The acquisition is conducted with a multichannel layout of vertical low-frequency geophones (2-4.5 Hz) and a shock source in an off-end pattern (MASW) or without active source (ReMi). In deeper investigations, a number of 3-component seismographs (10-30 s) is used in an array form (microtremor array). The common approaches used for deriving the dispersion curve from passive-source can be classified to two main families (Wathelet et al., 2004): frequency-wave number (Lacoss et al., 1969; Capon, 1969; Kvaerna and Ringdahl, 1986; Ohrnberger, 2001) and spatial auto-correlation (Aki, 1957; Roberts and Asten, 2004). As for active-source surface-wave methods, there are several algorithms for generating images of phase velocity dispersion energy: the F-K transformation (Yilmaz, 1987), the Tau-p transform (McMechan and Yedlin, 1981), the phase shift (Park et al., 1998), the slant stacking (Xia et al., 2007), and high-resolution Radon transform (Luo et al., 2009).

In the third stage, the dispersion curve is inverted to obtain V_S (and eventually V_P) vertical profiles, as in the classical active-source methods (Stokoe

et al., 1989; Malagnini et al., 1995). Compared with these latter methods, noise-based techniques offer the following advantages (Satoh et al., 2001): (i) being easily applied in urban areas; (ii) not requiring artificial seismic sources; (iii) allowing for greater depths to be reached (from tens of meters to hundreds of meters according to the array aperture and the noise-frequency content). Similar to all surface-wave methods, the obtained V_S profile is purely one-dimensional and is averaged within the array (Socco et al., 2010). This indicates that the technique is not appropriate when lateral variations are present.

For performing inversion, four challenges are encountered: the method of forward modeling, initial models, importance of higher modes, and choice of proper inversion algorithm (e.g., Socco et al., 2010). The inverse problem is usually solved with linearized algorithms that use a 1D forward model and yield a 1D S-wave velocity profile (Socco et al. 2010).

The important distinction in local search methods (LSMs) and global search methods (GSMs) is in between. The former one minimizes the misfit between the experimental and synthetic dispersion curve, starting from an initial velocity model and searching its vicinity; the latter one explores the solution space systematically (Socco et al., 2010).

Global search methods have been popular as they avoid all assumptions of linearity between the observable and the unknown, and offer a way of handling the non-uniqueness problem and its consequences (Cercato, 2009; Foti et al., 2009). However, GSMs require greater computing effort because multiple simulations must be performed to adequately sample the model parameter space. Several optimization methods have been applied over the years to make GSMs affordable. These methods use random generation of model parameters, but they can guide their search using a transition probability rule, e.g., simulated annealing (SA), on the basis of the Metropolis algorithm (Metropolis et al., 1953); or, they can apply genetic algorithms (GA) or an important sampling method (Sen and Stoffa, 1996). These approaches reduce the number of required simulations and sampling concentrated on the high-probability-density regions of the model parameter space. A number of examples for GSM applications can be found for surface wave inversion. The genetic algorithm has also been applied at different scales in numerous studies (e.g., Yamanaka and Hishida, 1996; Pezeshk and Zarrabi, 2005; Dal Moro et al., 2007). Beaty et al. (2002) and Pei et al. (2007) have used simulated annealing methods for geotechnical characterization to a depth of 10 m using fundamental and higher modes. Also, the neighborhood algorithm of Sambridge (1999), which can be considered an important sampling method, was adopted by Wathelet et al. (2004) to invert dispersion curves retrieved from noise measurements at seismologic scale. Socco and Boiero (2008) proposed an improved Monte Carlo approach that used non-dimensionalization of the forward problem of Rayleigh-wave propagation

to optimize sampling of the model space and a statistical test to draw inferences from the final results. Maraschini and Foti (2010) proposed a Monte Carlo multimodal inversion of surface waves.

As a disadvantage to GSMs, the final result is not a single V_S profile but is a set of acceptable V_S models. This result, even though more rigorous and consistent with non-uniqueness of the solution, is not easy to handle.

In this paper, the focus was on GSMs algorithm. Development of GSMs was done due to the following problems:

1. Reducing risk of being trapped in local minima.
2. Noisy dispersion curves, especially in the case of passive methods (microtremors).

Here a new code was developed using hybrid mutation particle swarm Optimization (called MPSO) algorithm. Particle swarm optimization (PSO) is a population-based stochastic optimization algorithm, first introduced by Kennedy and Eberhart (1995). It is a metaphor of the social behavior of animals, such as bird flocking and fish schooling. Comparing with other population-based stochastic optimization methods, such as Genetic Algorithms (GA) and Evolutionary Programming (EP), PSO has comparable or even superior search performance for many hard optimization problems with fast and stable convergence rate (Kennedy and Eberhart, 2001). It has already been applied with success to many scientific areas. However, PSO exhibits some disadvantages: sometimes there is a high possibility for this to be trapped in local optima (i.e., premature convergence), and the convergence rate decreased considerably in a later period of evolution (Gao and Xu, 2011). Mutation operators are an integral part of evolutionary computation techniques and preventing loss of diversity in a population of solutions. This allows a greater region of the search space to be covered. Furthermore, mutation operators introduce new individuals into a population by creating a variation of a current individual, thus adding variability into the population and preventing stagnation of the search in local optima (Dumitrescu et al., 2000). Therefore, the addition of mutation operator to PSO enhances its global search ability and thus improves its performance.

METHODOLOGY

Particle Swarm Optimization

Swarm Intelligence (SI) is a novel distributed intelligent paradigm for solving optimization problems and has originally taken its inspiration from the biological examples by swarming, flocking and herding phenomena in

vertebrates. Particle swarm optimization (PSO) incorporates swarming behaviors observed in flocks of birds, schools of fish, swarms of bees and even human social behavior, from which the idea is emerged (Kennedy and Eberhart, 2001; Clerc and Kennedy, 2002). PSO is a population-based optimization tool, which could be implemented and applied easily to solve various function optimization problems. In terms of the algorithm, an important feature of PSO is its algorithmic simplicity and fast convergence (Lu et al., 2010), which is favorably compared with many global optimization algorithms, such as genetic algorithms (Goldberg, 1989), simulated annealing (Triki et al., 2005) and other global optimization algorithms. Feasible implementation of PSO depends on appropriately mapping the problem solution into the PSO particle (Eberhart and Kennedy, 1995).

The particles in PSO consist of a D-dimensional position vector $\mathbf{x}_i$, and a D-dimensional velocity vector $\mathbf{v}_i$; so, the i-th member of a population's position is represented as $\mathbf{x}_i = [x_{i1},x_{i2},\ldots,x_{iD}]$ and its velocity as $\mathbf{v}_i = [v_{i1},v_{i2},\ldots,v_{iD}]$. The PSO algorithm begins by randomly initializing a population of these particles and then iteratively evaluating and updating them until finding better solutions. The particle update method tries to move particles to better positions by accelerating them towards their own previous best solution which has been achieved so far, as the factor *pbest*, and the best solution achieved by any particle in its neighborhood, as the factor *nbest*. So for the i-th member of a population, the *pbest* is represented by vector $\mathbf{p}_i = [p_{i1},p_{i2},\ldots,p_{iD}]$ and the *nbest* as $\mathbf{p}_n = [p_{n1},p_{n2},\ldots,p_{nD}]$, where n is the particle index of the best neighbor of i. Original particle update equations of Eberhart and Kennedy (1995) have been improved in a number of studies. Eberhart and Shi (2000) stated that the best approach was to use the constriction factor method of Clerc (1999), which investigated use of a parameter called constriction factor K inspired by the earlier work on the use of an inertia weight by Shi and Eberhart (1998). Using the constriction factor, the particle velocity dimensions are updated via:

$$v_{id}(t) = K[v_{id}(t-1) + c_1r_1\{p_{id}-x_{id}(t-1)\} + c_2r_2\{p_{nd}-x_{id}(t-1)\} \quad , \qquad (1)$$

$$K = 2/|2 - \varphi - \sqrt{(\varphi^{-2}-4\varphi)}| \quad , \quad \varphi = c_1 + c_2, \ \varphi > 4. \qquad (2)$$

With the particle position dimensions being updated via the original equation of Eberhart and Kennedy (1995):

$$x_{id}(t) = x_{id}(t-1) + v_{id}(t) \quad . \qquad (3)$$

Here, t is the current algorithm iteration, c_1 and c_2 are two positive constants and r_1 and r_2 are two separately generated random numbers in a uniform range [0:1]. Typically, values of 2.05 are used for c_1 and c_2, making $\varphi = 4.1$ and $K = 0.729$. These equations have the effect of accelerating particles toward the weighted sum of the *pbest* and *nbest* positions with an element of randomness.

There are two main versions of the PSO algorithm called local and global ones, which differ in the way the particle neighborhoods are defined. In the global version, a particle's neighborhood consists of all other particles, whereas in the local version, a particle's neighborhood is a subset of other particles. This neighborhood is defined as topological neighbors in the particle array and does not change during the algorithm's run. So for a neighborhood size of 3, neighbors of particle i are particles $i-1$, i and $i+1$. In both of these versions, the *gbest* denotes the best solution of any particle in the population. The benefit of a local version is that it is more resistant to getting stuck in local minima; but, it is generally slower to converge. For further details, the reader can refer to Kennedy and Eberhart (2001).

Hybrids of the PSO algorithm have also been produced by introducing ideas from evolutionary computation techniques such as selection (Angeline, 1998) and mutation operators, which are to be discussed in the next section.

Mutation Based Particle Swarm Optimization (MPSO)

The behavior of PSO in the *gbest* model presents some important aspects related to the velocity update. If a particle's current position coincides with the global best position, the particle will only move away from this point if its inertia weight and previous velocity are different from zero. If their previous velocities are very close to zero, then all the particles will stop moving once they catch up with the global best particle, which may lead to a premature convergence of the algorithm. In fact, this does not even guarantee that the algorithm has converged on a local minimum. It means that all the particles have converged at the best position discovered so far by the swarm. This phenomenon is known as stagnation (Esmin et al., 2005; Esmin et al., 2006). Like evolutionary computation techniques, Ratnaweera et al. (2004) stated that lack of population diversity in PSO algorithms was understood as a factor in their convergence on local minima. Therefore, addition of a mutation operator to PSO could enhance its global search capacity and thus improve its performance.

We included the mutation process used in GA into PSO and by varying the mutating space along the search. The stagnation is assuaged by this technique and introduces diversity into the population. This process allows the swarm to escape from the local optima and to search in different zones of the search space. As a result, the proposed algorithm has the automatic balance ability between global and local searching abilities and achieves better convergence.

This process starts with the random choice of a particle in the swarm and moves to the different positions inside the search area. During every iteration,

the population is divided into two parts: the first is generated according to a population-based transition rule and the second is generated by a proposed mutation-based scheme. Note that, the main part is the population-based section. The reason for employing the second part is to avoid convergence in a local minima solution. As the number of iteration is increased, PSO leads to fast convergence in a non-optimal (non near-optimal) solution. So, having a more population-based one is preferred at the beginning; as the iteration number is increased, the mutation-based population will be raised. In this way, a percentage of the mutation-based part is represented by PPm, which increases linearly from PPm_{min} to PPm_{max} during the execution of the algorithm that is tuned as eq. (4). It_{max} is the maximum number of iteration and It is the current iteration. We set the PPm_{min}, PPm_{max} and It_{max} as 0.05, 0.5 and 50, respectively, in this study.

$$PPm_i = PPm_{min} + (It/It_{max})(PPm_{max} - PPm_{min}) \quad . \tag{4}$$

By applying the mutation process, the particle moves to the other side in the space. This prevents the particles from being trapped in the local minima. Fig. 1 lists the pseudo-code for the basic MPSO algorithm.

```
Begin
Create an initialize:

    While (stop condition is false)
    Begin

        Evaluation
        Update velocity and position
        Mutation

    End
End
```

Fig. 1. The pseudo code for MPSO algorithm.

MPSO for surface wave analysis

The experiments were tested on an Intel PC with 1.7 GHz processor and 2 GB memory running MATLAB R2009a in Windows XP. The experiments were carried out on the models (Tables 1, 3). For tuning the parameters, different values were tested and the best values were considered for each algorithm. The population size and max-iteration for MPSO were set to the same values of 50 and 50, respectively.

The codes we developed here aims at performing nonlinear inversion of fundamental-mode and/or higher-mode Rayleigh-waves using a MPSO strategy. In the current research, the focus was on inversion results of fundamental-mode and first high-mode Rayleigh-wave dispersion curves for near-surface S-wave, P-wave velocities and layer thicknesses. Rayleigh-wave dispersion is dominated by S-wave velocity and thicknesses (Xia et al., 1999) but since in Rayleigh-wave dispersion P-wave plays a minor but not completely negligible role (please notice that in porous media P-wave values are strongly affected by the water content and are then subject to large variations), Poisson values are free to vary around a value and by a percentage which the user can define (Dal Moro et al., 2011). The inversion was done for S-wave and P-wave velocities by the assumption of ($0.2 <$ Poisson's ratio < 0.5) and fixing densities to their known values.

To fully evaluate the capability of the proposed inversion strategy and simulate more realistic cases in which no prior information is available, a wider search scope of the solution space was used. The lower and upper limits of the search areas departed 50% or more from their true values in all of the latter tests. As presented by Xia et al. (2003), the best match with the measured data does not necessarily result in the best inversion results. Here, after a few runs of MPSO we set the number of iterations to 50 for noise-free, contaminated, and field data.

The forward modeling of Rayleigh-wave dispersion curves is based on the fast Dunkin's (1965) formulae algorithm developed by Wathelet et al. (2004), who used an efficient root search based on the Lagrange polynomial which was constructed by iteration with Neville's method (Press et al., 1992). The procedure was designed to find the global minimum of RMS (root-mean-square) error misfit between the measured and predicted phase velocities. The objective function was defined as (Dal Moro et al., 2007):

$$\text{misfit} = \left\| V_R^{obs} - V_R^{theo} \right\|_2 / \sqrt{m} \quad , \tag{5}$$

where V_R^{obs} is an $m \times 1$ vector of the observed Rayleigh-wave phase velocities, V_R^{theo} is an $m \times 1$ vector of the theoretical Rayleigh-wave phase velocities and m is the number of dispersion points (phase velocities versus frequency).

SYNTHETIC DATA INVERSION

Example 1: The two-layer model

In the first example presented here, a simple earth model consisting of a homogeneous single layer overlying a half-space was used. This example was performed to test the efficiency and stability of MPSO. The model A with different velocity contrasts was used in this section (see Table 1 for more details). Here a frequency range of 1-30 Hz with 50 samples was utilized for computing noise-free synthetic dispersion curve for this model. Also prior to applying MPSO to Rayleigh-wave dispersion curves, different types of initialization were chosen:

1. Joint inversion S-wave, P-wave velocities and thickness by the assumption of (0.2 < Poisson's ratio < 0.5) by selection of search space departing 50% true values.

2. Adding 10% Gaussian noise to dispersion curve due to the step one conditions.

3. Joint inversion of fundamental and first higher modes of Rayleigh-wave dispersion curves due to the step one conditions.

Table 1. Benchmark model to evaluate calculation efficiency and stability of MPSO.

	Layer	Thickness (m)	50% Search Space	V_P (m/s)	50% Search Space	V_S (m/s)	50% Search Space	Density (kg/m^3)
Model A	1	30	15-45	500	250-750	200	100-300	1800
	2	Half-space		1600	800-2400	800	400-1200	2000

Three different disturbing of dispersion curve and initialization was performed using the MPSO algorithm. Standard deviation (SD) and average relative error (RE %) between the true models and models estimated from MPSO inversions, on three different data sets, are shown in Table 2.

Fig. 2 shows the inversion results of noise-free data for model A. A good agreement between measured and inverted dispersion curves can be seen here (see Fig. 2a). For this curve the average relative error for all parameters of model A (H_1,V_{S1},V_{S2}) are less than 1%. For this example we found the experimental surface wave phase velocities to be very noisy. Here, in order to investigate the effect of noise inclusion on the surface wave data and also to examine the vulnerability of our algorithm, 10% white Gaussian noise was added to the dispersion curve. For this scenario, the inversion results show more

relative error in model parameters, and higher misfit values were observed relative to the free-noise data. Also as shown in Fig. 3, the inversion results were acceptable for this case. The misfit function was also computed. Fig. 4. compares the misfit function between the noise-free data and the data calculated for the situation wherein 10% noise was added. It is seen here that the misfit function for the noise-free run (shown as dots in Fig. 4.) rapidly decreases in the first 20 iterations through the solution. Here, a minimum misfit value of approximately 10^{-3} was obtained after 50 iterations. As for the second run in which the white noise was added, the misfit decreases to approximately 10^{-1} after 5 iterations and then remains constant.

Joint inversion of fundamental and first higher modes of Rayleigh-wave dispersion curves could increase the reliability V_S and thickness results (relative error 0.0% for thickness and V_{S1}) (Fig. 5).

Table 2. MPSO inversion results and statistics of inversion results A.

Model A	True	model	SD	RE (%)
50% Search Space				
H_1(m)	30	29.8	0.67	0.67
V_{S1}(m/s)	200	200.5	1.35	0.25
V_{S2}(m/s)	800	803.3	14.31	0.41
50% Search Space with 10% Gaussian noise				
H_1(m)	30	29.4	0.84	2.00
V_{S1}(m/S)	200	200.7	1.49	0.35
V_{S2}(m/S)	800	779.6	7.69	2.55
50% Search Space Joint with First Higher Mode				
H_1(m)	30	30.0	0.00	0.00
V_{S1}(m/S)	200	200	0.0	0.00
V_{S2}(m/S)	800	812.1	6.52	1.51

Example 2: The five-layer model

The second example presented in this study investigates the efficiency and stability of MPSO for three distinct models. The first model, indicated as model B, consists of five-layer model in which S-wave velocities increase with depth. The second model, indicated as model C, considered the same layers wherein a soft layer is trapped between two stiff layers. For the third model, namely model D, presented here there are five-layer too with a stiff layer sandwiched between two soft layers (Table 3). Here for each model, a frequency range of 0.5-30 Hz with 50 samples was utilized for computing a noise-free synthetic dispersion curve. Different types of initialization were chosen as the same as example 1. For each model Standard Deviation (SD) and average relative error (RE %) between true models and models estimated from MPSO inversions on three different data are shown in Table 4.

Table 3. Benchmark model to evaluate calculation efficiency and stability of MPSO.

	Layer	Thickness (m)	50% Search Space	Vp (m/s)	50% Search Space	Vs (m/s)	50% Search Space	Density (kg/m3)
Model B	1	20	10-30	600	300-900	200	100-300	1800
	2	10	5-15	900	450-1350	300	150-450	1900
	3	30	15-45	1200	600-1800	400	200-600	1900
	4	50	25-75	1800	900-2700	600	300-900	2000
	5	Half-space	------	3000	1500-4500	1000	500-1500	2100
Model C	1	10	5-15	600	300-900	200	100-3--	1800
	2	20	10-30	450	225-675	150	75-225	1900
	3	30	15-45	900	450-1350	300	150-450	1900
	4	50	25-75	1500	750-2250	500	250-750	2000
	5	Half-space	------	2400	1200-3600	800	400-1200	2100
Model D	1	10	5-15	450	225-675	150	75-225	1800
	2	20	10-30	750	375-1125	250	125-375	1900
	3	30	15-45	600	300-900	200	100-300	1900
	4	50	25-75	1500	750-2250	500	250-750	2000
	5	Half-space	------	2400	1200-3600	800	400-1200	2100

Table 4. MPSO inversion results and statistics of inversion results B, C & D.

Model	True	model	SD	RE (%)
Model B) Fundamental Mode				
H_1(m)	20	19.6	2.6	1.75
H_2(m)	10	10.2	2.4	2.40
H_3(m)	30	31.2	6.8	4.17
H_4(m)	50	48.2	14.7	3.60
V_{s1}(m/s)	200	200.4	0.8	0.20
V_{s2}(m/s)	300	312.7	36.8	4.23
V_{s3}(m/s)	400	407.2	27.3	1.80
V_{s4}(m/s)	600	625.8	34.9	4.30
V_{s5}(m/s)	1000	1005.2	7.9	0.53
Model B) Fundamental Mode with 10% Gaussian noise				
H_1(m)	20	20.9	2.2	4.50
H_2(m)	10	10.6	4.3	6.00
H_3(m)	30	29.5	10.0	1.67
H_4(m)	50	55.3	18.3	10.60
V_{s1}(m/s)	200	200.1	0.6	0.05
V_{s2}(m/s)	300	343.9	74.9	14.63
V_{s3}(m/s)	400	404.9	51.1	1.22
V_{s4}(m/s)	600	625.4	106.3	4.23
V_{s5}(m/s)	1000	1026.9	26.9	2.69
Model B) Joint with First Higher Mode				
H_1(m)	20	20.1	1.1	0.56
H_2(m)	10	9.9	2.7	1.00
H_3(m)	30	29.4	6.3	1.85
H_4(m)	50	49.3	8.1	1.33
V_{s1}(m/s)	200	200.1	0.9	0.05
V_{s2}(m/s)	300	297.3	45.4	0.90
V_{s3}(m/s)	400	405.8	24.9	1.45
V_{s4}(m/s)	600	627.8	32.2	4.63
V_{s5}(m/s)	1000	1005.7	15.0	0.57

Model	True	model	SD	RE (%)
Model C) Fundamental Mode				
H_1(m)	10	9.3	2.9	7.00
H_2(m)	20	21.2	1.4	6.00
H_3(m)	30	28.6	8.7	4.44
H_4(m)	50	41.5	14.7	16.89
V_{s1}(m/s)	200	216.5	33.8	8.25
V_{s2}(m/s)	150	150.4	0.5	0.27
V_{s3}(m/s)	300	328.6	58.7	9.53
V_{s4}(m/s)	500	472.4	79.9	5.51
V_{s5}(m/s)	800	824.3	21.2	3.04
Model C) Fundamental Mode with 10% Gaussian noise				
H_1(m)	10	9.1	3.4	9.00
H_2(m)	20	18.2	2.3	9.00
H_3(m)	30	30.1	8.6	0.33
H_4(m)	50	44.3	15.4	11.40
V_{s1}(m/s)	200	221.3	37.3	10.65
V_{s2}(m/s)	150	151.4	12.5	0.93
V_{s3}(m/s)	300	271.3	76.7	9.57
V_{s4}(m/s)	500	663.5	76.5	32.70
V_{s5}(m/s)	800	788.1	23.3	1.49
Model C) Joint with First Higher Mode				
H_1(m)	10	9.8	0.9	2.00
H_2(m)	20	20.3	1.3	1.50
H_3(m)	30	30.1	6.9	0.37
H_4(m)	50	41.2	6.1	17.60
V_{s1}(m/s)	200	207.4	21.5	3.70
V_{s2}(m/s)	150	149.9	0.6	0.07
V_{s3}(m/s)	300	303.3	20.2	1.10
V_{s4}(m/s)	500	494.1	89.6	1.18
V_{s5}(m/s)	800	809.1	24.9	1.14

Model	True	model	SD	RE (%)
Model D) Fundamental Mode				
H_1(m)	10	10.1	0.6	1.82
H_2(m)	20	19.7	6.4	1.50
H_3(m)	30	31.5	6.6	5.15
H_4(m)	50	39.4	13.4	21.09
V_{s1}(m/s)	150	151.0	1.7	0.73
V_{s2}(m/s)	250	276.1	26.7	10.47
V_{s3}(m/s)	200	199.4	14.1	0.27
V_{s4}(m/s)	500	549.2	163.7	9.84
V_{s5}(m/s)	800	815.3	25.1	1.92
Model D) Fundamental Mode with 10% Gaussian noise				
H_1(m)	10	10.0	1.8	0.00
H_2(m)	20	17.7	5.2	11.50
H_3(m)	30	31.8	7.1	6.00
H_4(m)	50	35.1	16.4	29.80
V_{s1}(m/s)	150	149.0	8.5	0.67
V_{s2}(m/s)	250	270.7	22.6	8.28
V_{s3}(m/s)	200	203.8	24.4	1.90
V_{s4}(m/s)	500	612.5	132.4	22.50
V_{s5}(m/s)	800	825.2	24.4	3.15
Model D) Joint with First Higher Mode				
H_1(m)	10	10.0	0.0	0.00
H_2(m)	20	19.1	1.5	4.55
H_3(m)	30	31.2	2.0	4.07
H_4(m)	50	50.1	19.0	0.18
V_{s1}(m/s)	150	149.9	0.3	0.06
V_{s2}(m/s)	250	255.3	2.8	2.11
V_{s3}(m/s)	200	201.2	1.8	0.59
V_{s4}(m/s)	500	537.4	73.6	7.48
V_{s5}(m/s)	800	810.6	15.9	1.32

Figs. 6 to 8 show the inversion results of MPSO on noise-free fundamental mode of dispersion curve for model B, model C, and model D, respectively. A good agreement was found between V_{S1} and the inversion results for all models. In model B (see Fig. 6) with increasing V_{S1} layers, the relative error and standard deviation were higher than that of the simple two layer model. By comparing to model B, the results in model C (LVL) were remarkable (see Fig. 7); low relative error was shown for the low velocity layer in this model. Theoretically refraction method fails to find the low velocity layer

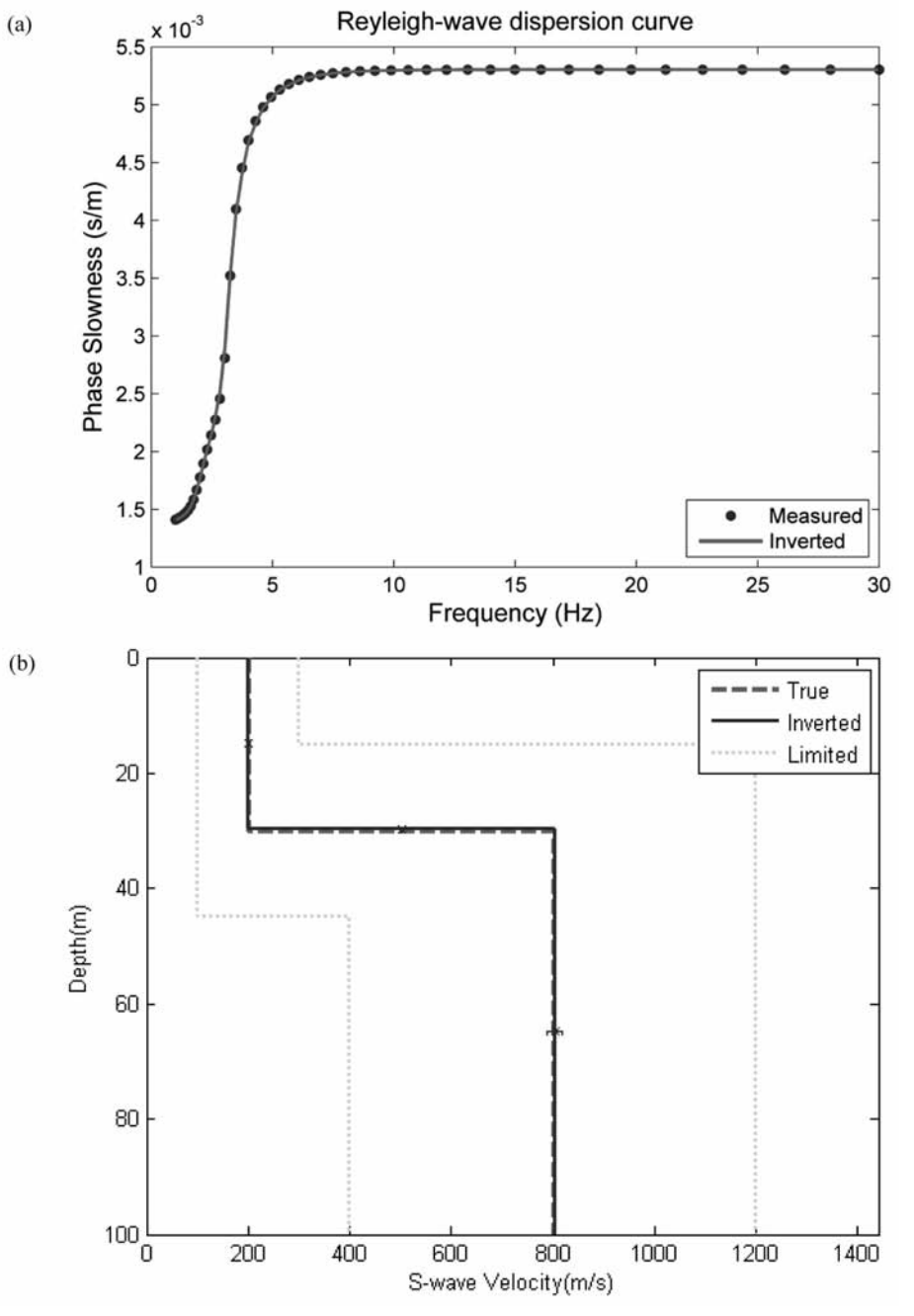

Fig. 2. Inversion of dispersion curve using MPSO for model A. (a) Noise free data (solid dots) and modeled dispersion curve (solid line). (b) The lower and upper bounds (50%) of the search area (dash-dots lines), true model (dashed line) and inverted S-wave velocity profile with standard deviation (solid line).

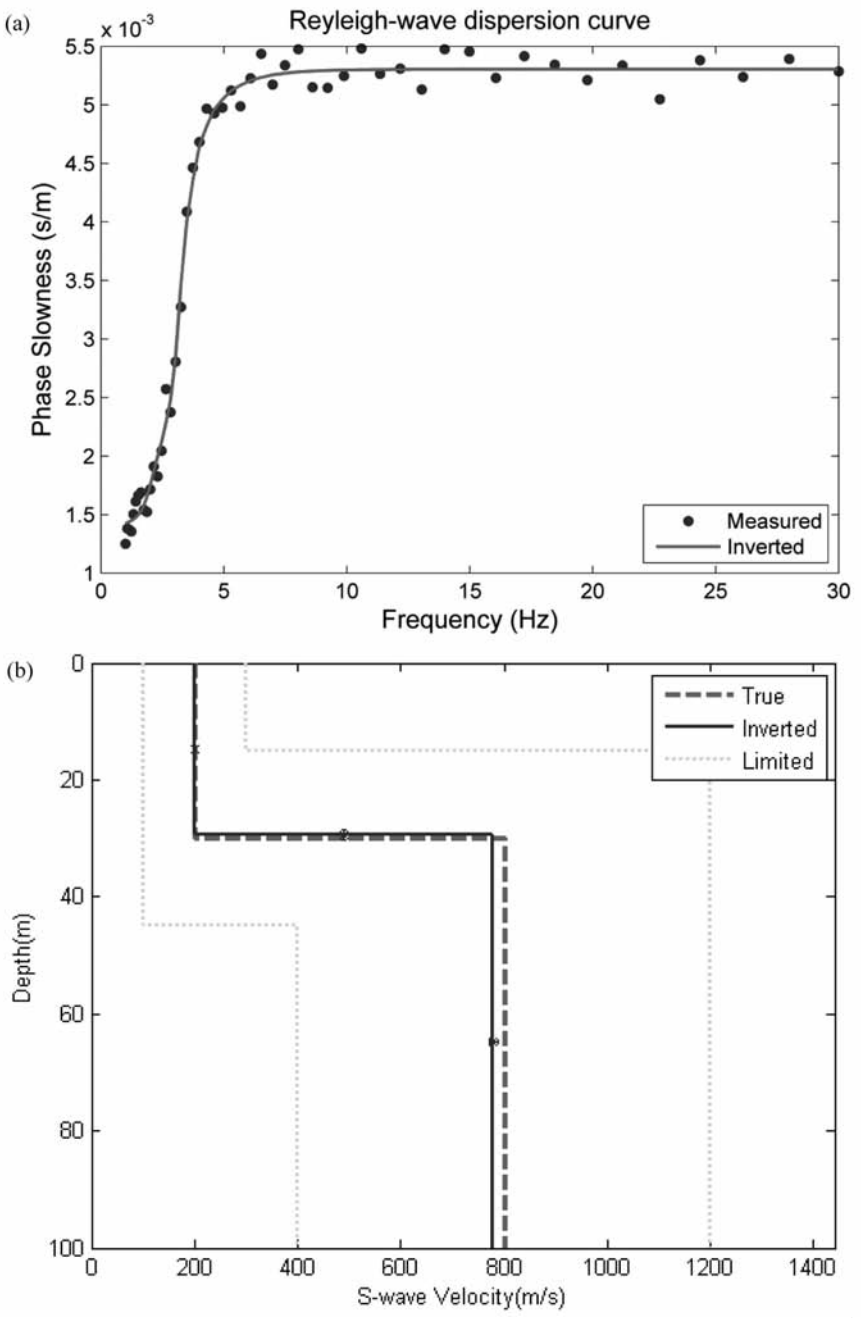

Fig. 3. Inversion results of Model using MPSO for model A. (a) Data with 10% white Gaussian noise (solid dots) and modeled dispersion curve (solid line). (b) The lower and upper bounds (50%) of the search area (dashed lines), true model (dotted line) and inverted S-wave velocity profile with standard deviation (solid line).

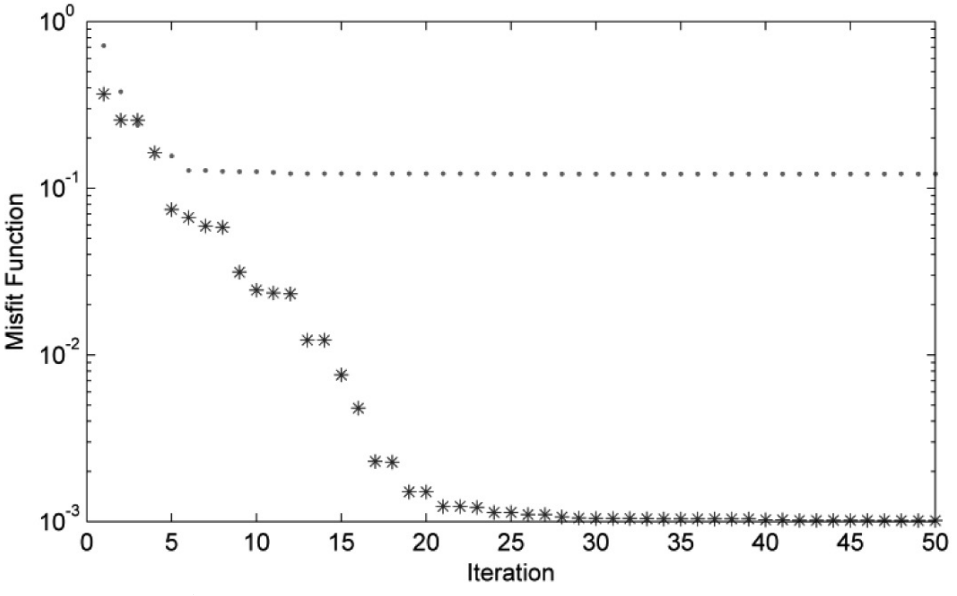

Fig. 4. Effects of inclusion of noise in surface wave dispersion data from Model A on performance of MPSO. Misfit function using noise-free data (solid stars) and Misfit function using 10% white Gaussian noise data (solid dots).

but in such a case (LVL), the surface wave inversion method can be more effective. This was obtained for the inversion performed for model D (see Fig. 8). Here for all models, the maximum relative error was observed in the forth layer. However, in all models, MPSO works as well as possible.

Figs. 9 to 11 show the inversion results of MPSO on noise-corrupted fundamental mode of dispersion curve for model B, model C, and model D, respectively. Similar to the noise-free data, the agreement between true models and inversion results obtained here are also good. The inversion results for all models (Figs. 9 to 11) show that the general velocity trend is properly identified. However, in comparison to the results for the noise-free data, a higher relative error was observed here. Here again the maximum errors are observed at layer 4 in each model. We recognize that MPSO algorithms are robust, not only in terms of accuracy but also in terms of computation effort, when applied to the surface wave inversion problem.

To improve the inversion results, we include the first higher mode and tested the results. Figs. 12 to 14 show the shear-wave vertical profiles for model B, model C, and model D, respectively. By comparing to the results obtained for the fundamental mode only (Figs. 6 to 8), an improvement of the inversion results with smaller relative error is observed.

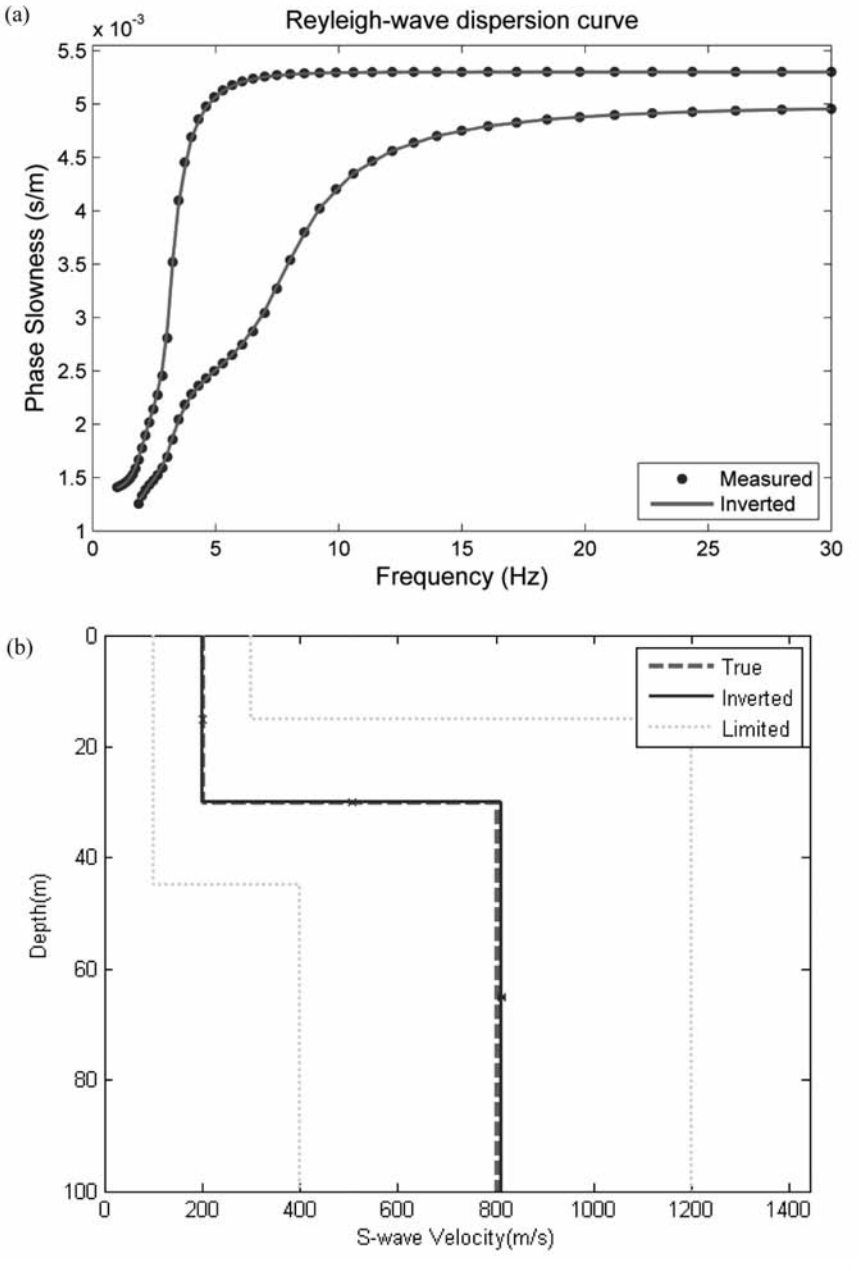

Fig. 5. Inversion of dispersion curve using MPSO for model A. (a) First higher mode (solid dots) and modeled dispersion curve (solid line). (b) The lower and upper bounds (50%) of the search area (dash-dots lines), true model (dashed line) and inverted S-wave velocity profile with standard deviation (solid line).

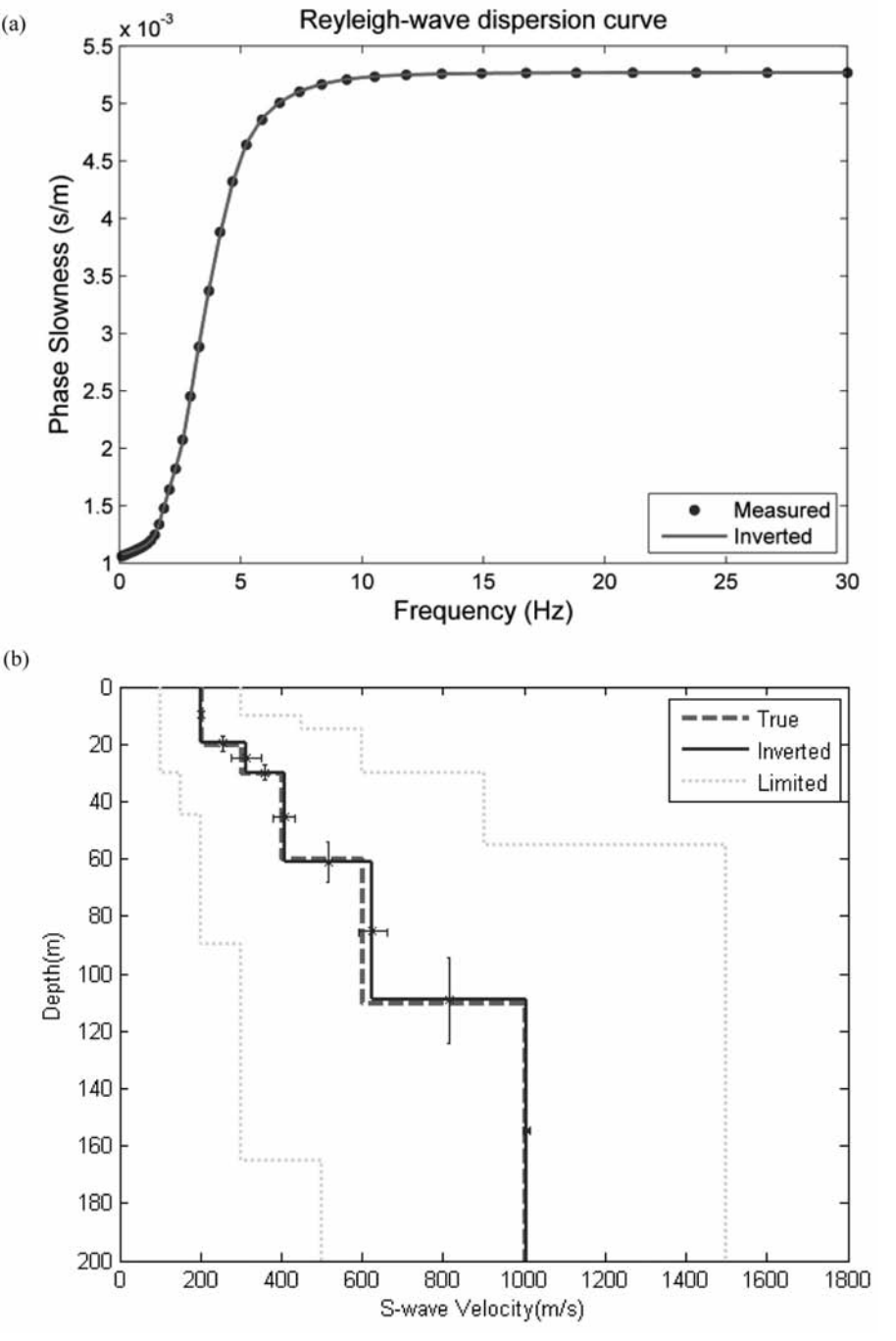

Fig. 6. Inversion of dispersion curve using MPSO for model B. (a) Noise free data (solid dots) and modeled dispersion curve (solid line). (b) The lower and upper bounds (50%) of the search area (dash-dots lines), true model (dashed line) and inverted S-wave velocity profile with standard deviation (solid line).

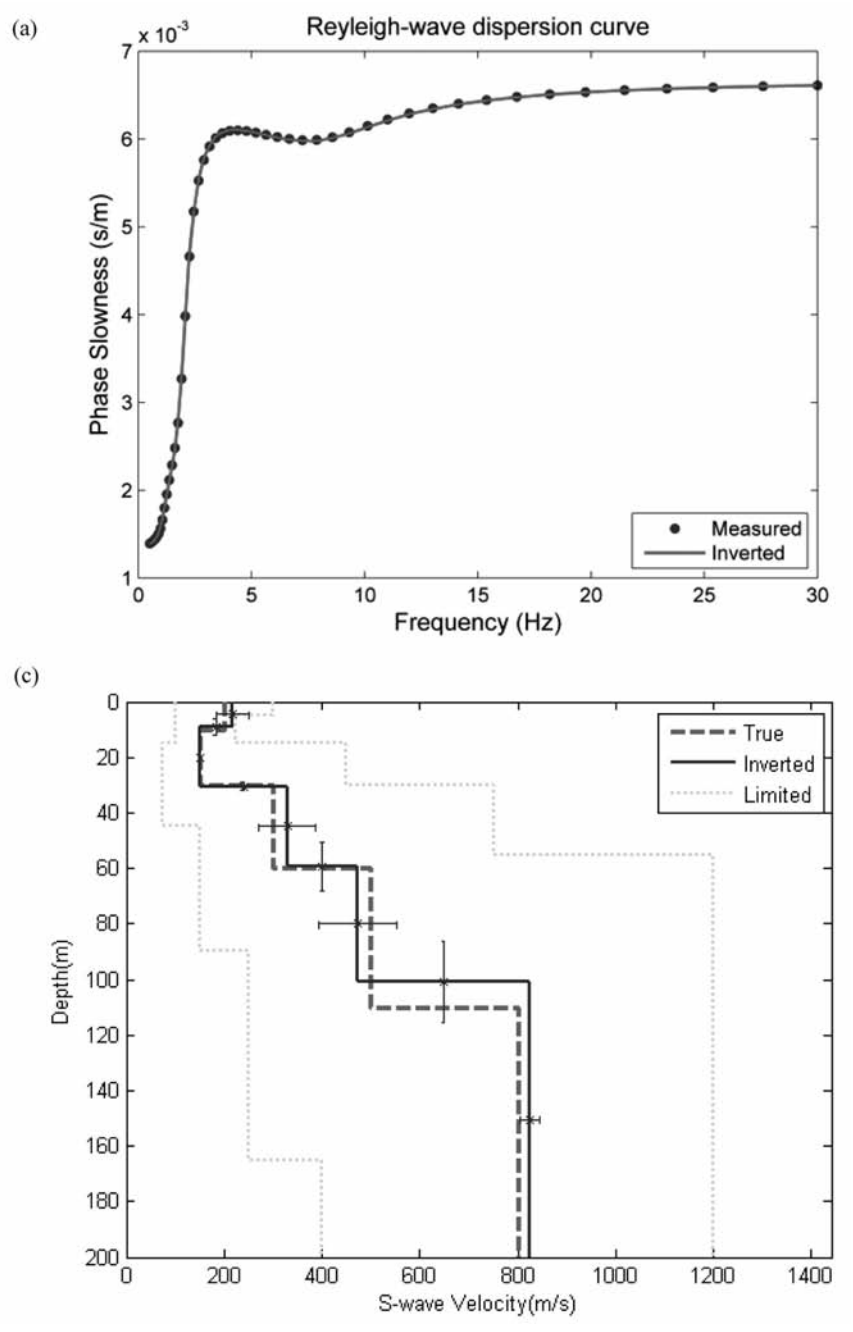

Fig. 7. Inversion of dispersion curve using MPSO for model C. (a) Noise free data (solid dots) and modeled dispersion curve (solid line). (b) The lower and upper bounds (50%) of the search area (dash-dots lines), true model (dashed line) and inverted S-wave velocity profile with standard deviation (solid line).

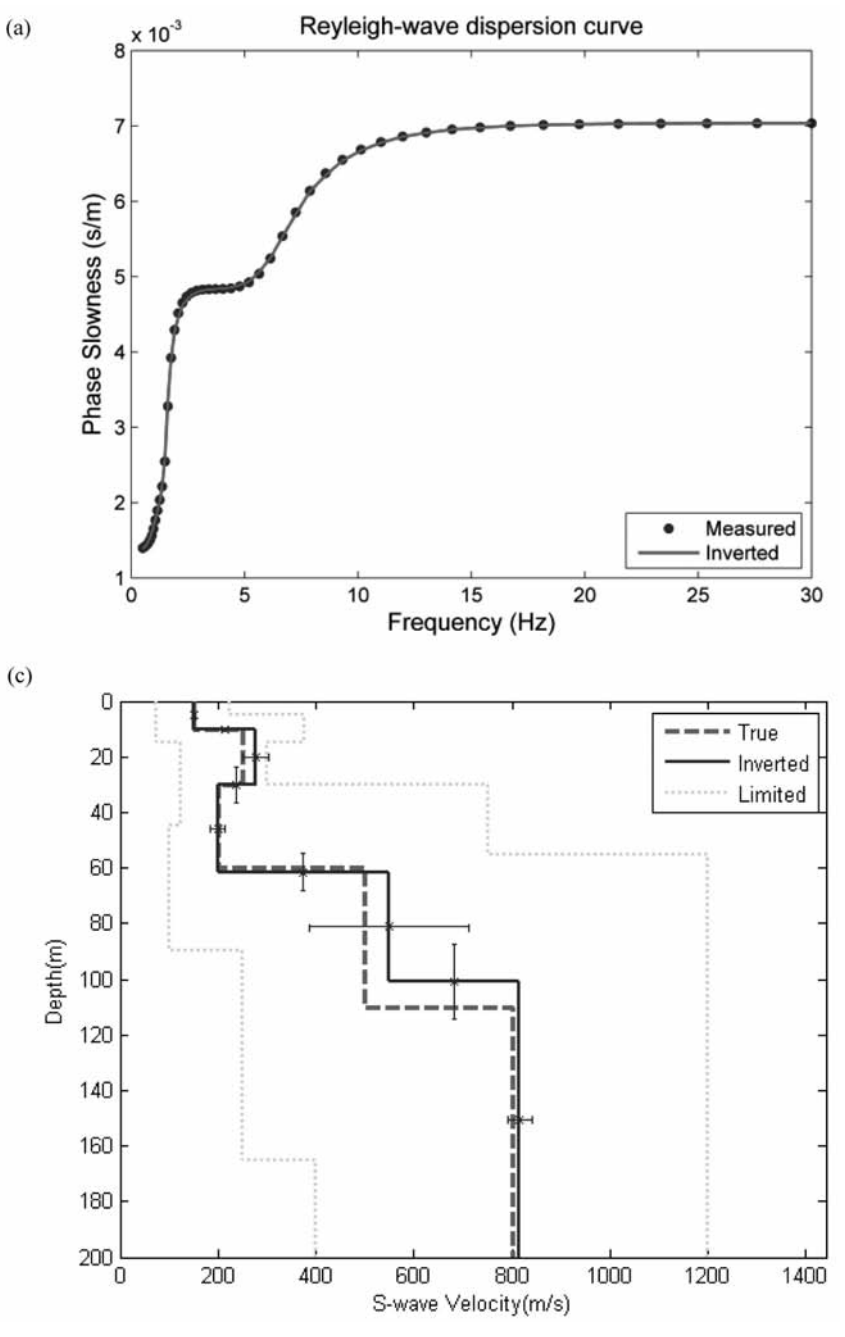

Fig. 8. Inversion of dispersion curve using MPSO for model C. (a) Noise free data (solid dots) and modeled dispersion curve (solid line). (b) The lower and upper bounds (50%) of the search area (dash-dots lines), true model (dashed line) and inverted S-wave velocity profile with standard deviation (solid line).

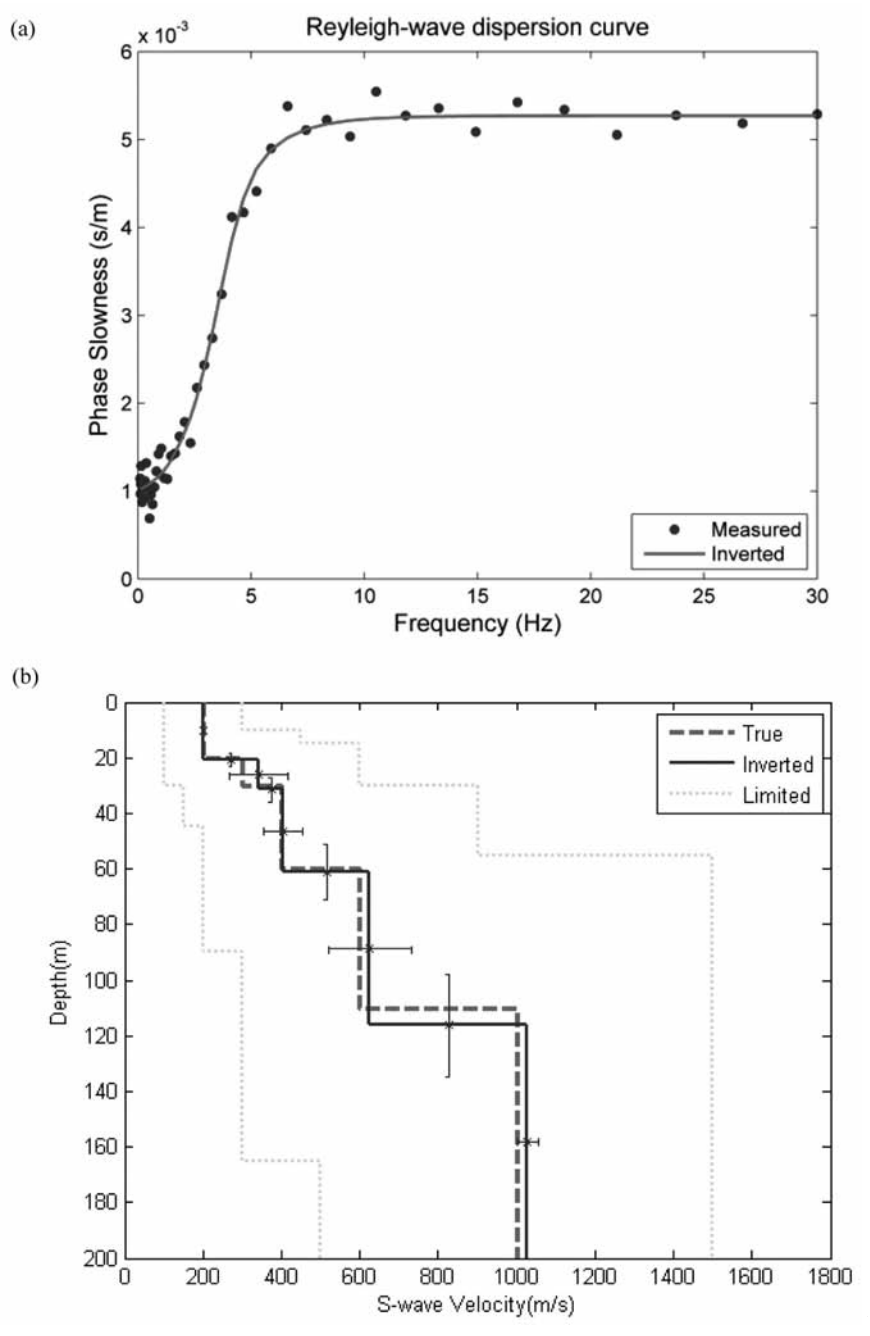

Fig. 9. Inversion results of Model using MPSO for model B. (a) Data with 10% white Gaussian noise (solid dots) and modeled dispersion curve (solid line). (b) The lower and upper bounds (50%) of the search area (dashed lines), true model (dotted line) and inverted S-wave velocity profile with standard deviation (solid line).

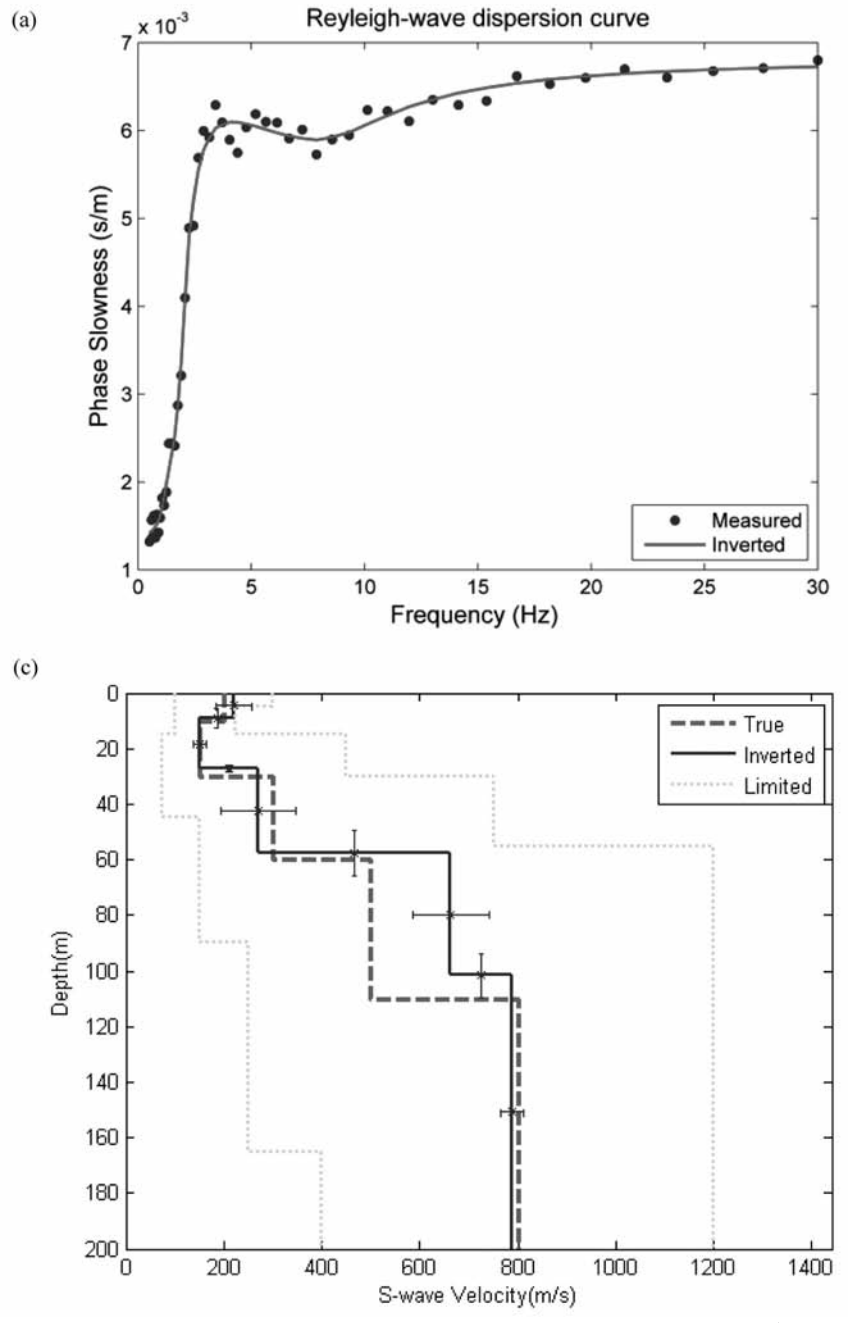

Fig. 10. Inversion results of Model using MPSO for model C. (a) Data with 10% white Gaussian noise (solid dots) and modeled dispersion curve (solid line). (b) The lower and upper bounds (50%) of the search area (dashed lines), true model (dotted line) and inverted S-wave velocity profile with standard deviation (solid line).

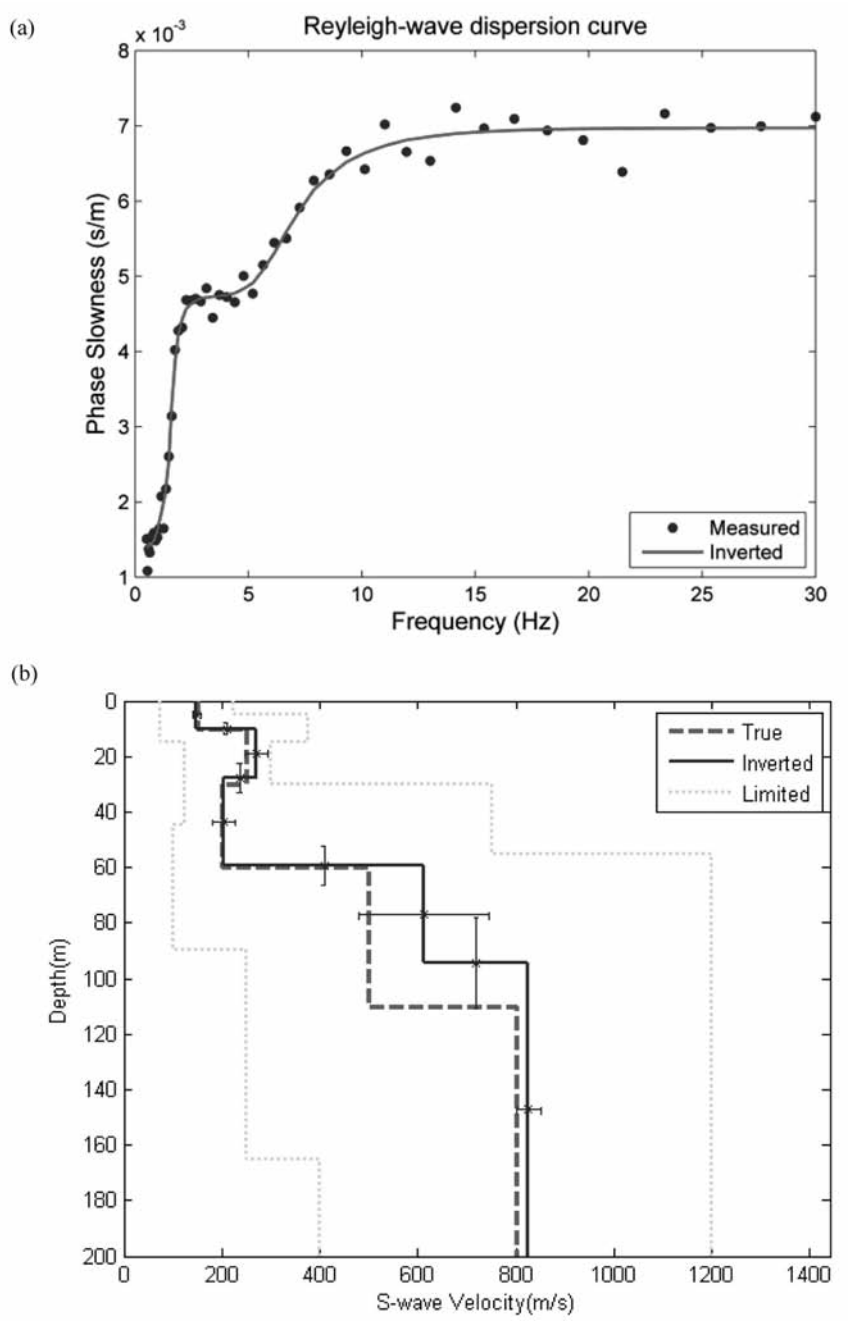

Fig. 11. Inversion results of Model using MPSO for model D. (a) Data with 10% white Gaussian noise (solid dots) and modeled dispersion curve (solid line). (b) The lower and upper bounds (50%) of the search area (dashed lines), true model (dotted line) and inverted S-wave velocity profile with standard deviation (solid line).

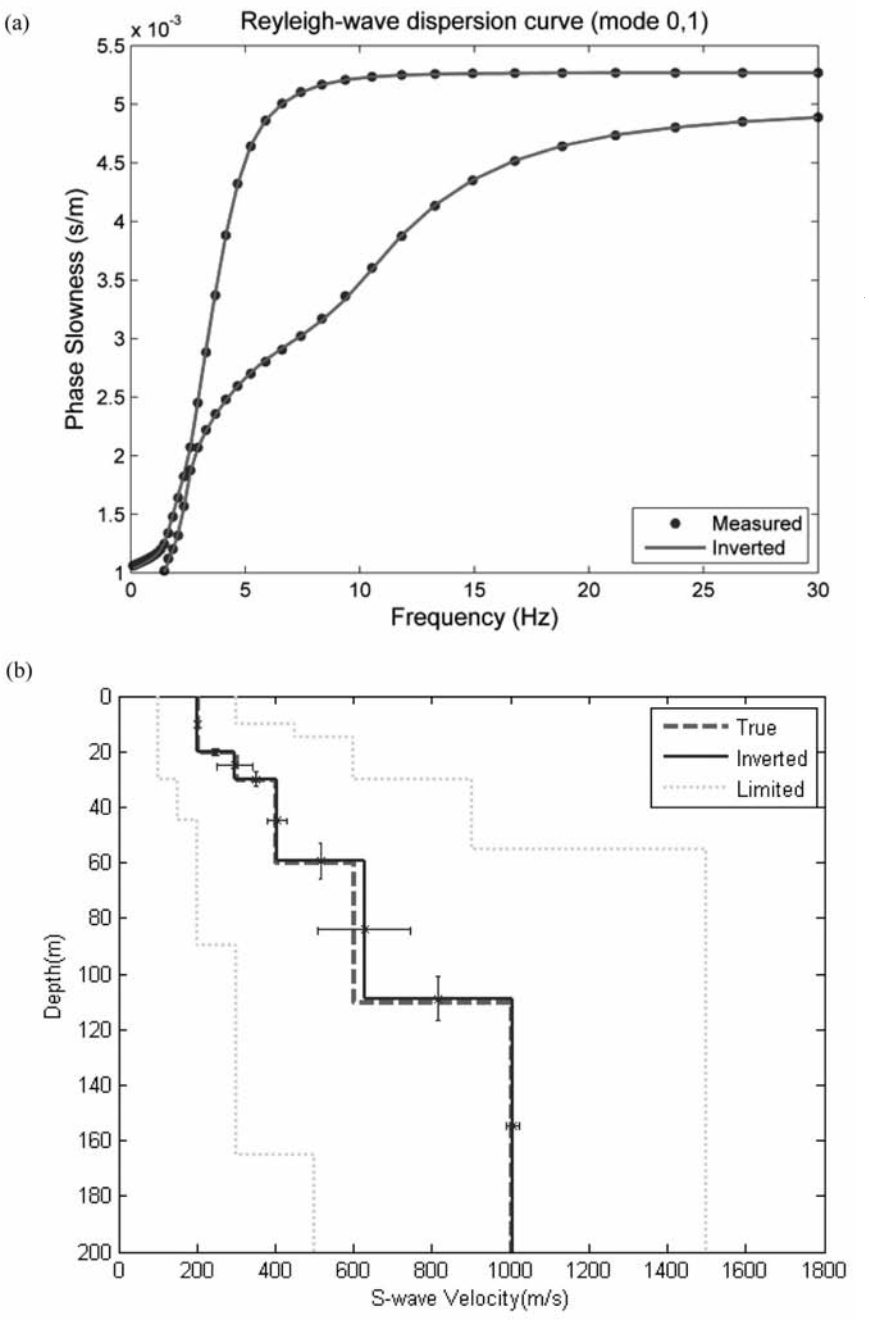

Fig. 12. Inversion of dispersion curve using MPSO for model B. (a) First higher mode (solid dots) and modeled dispersion curve (solid line). (b) The lower and upper bounds (50%) of the search area (dash-dots lines), true model (dashed line) and inverted S-wave velocity profile with standard deviation (solid line).

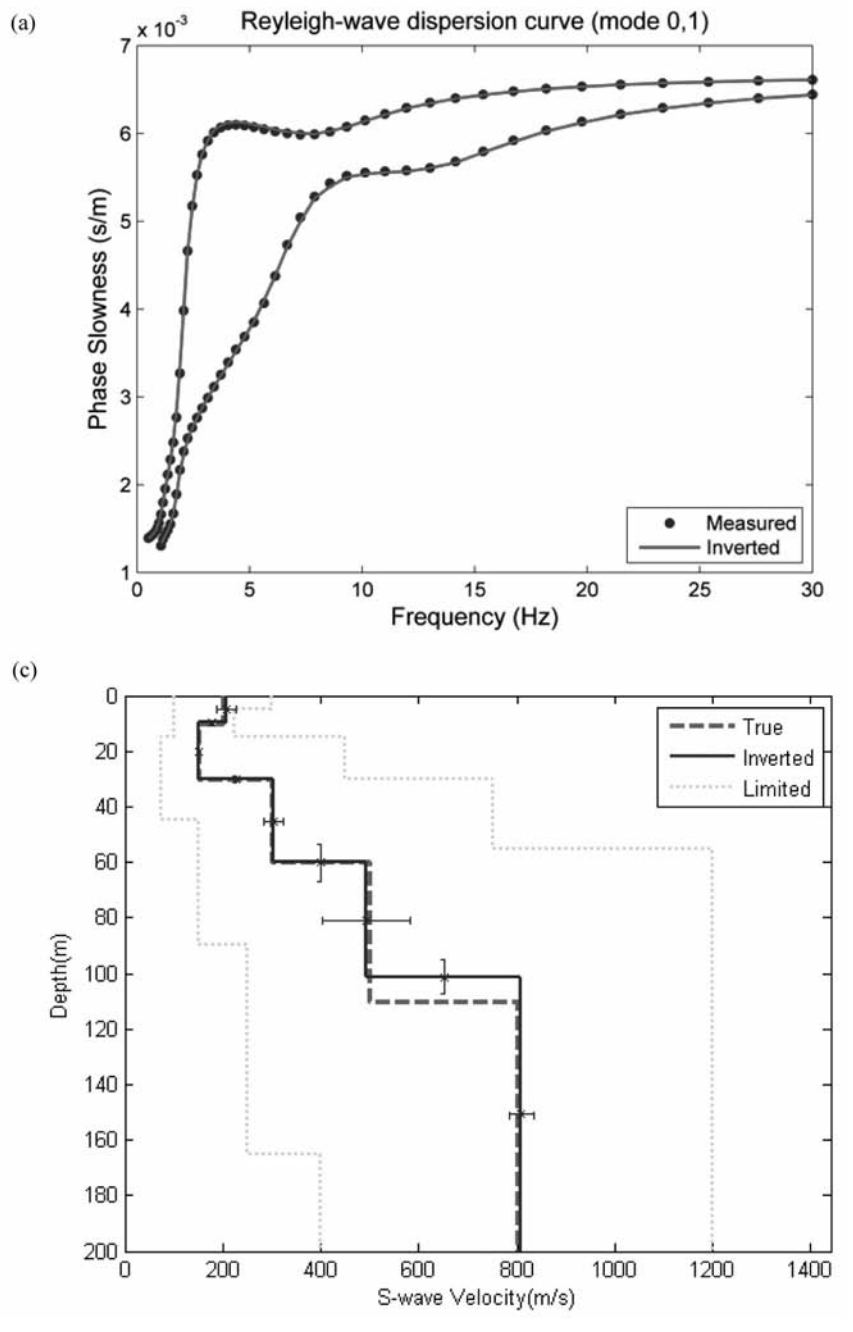

Fig. 13. Inversion of dispersion curve using MPSO for model B. (a) First higher mode (solid dots) and modeled dispersion curve (solid line). (b) The lower and upper bounds (50%) of the search area (dash-dots lines), true model (dashed line) and inverted S-wave velocity profile with standard deviation (solid line).

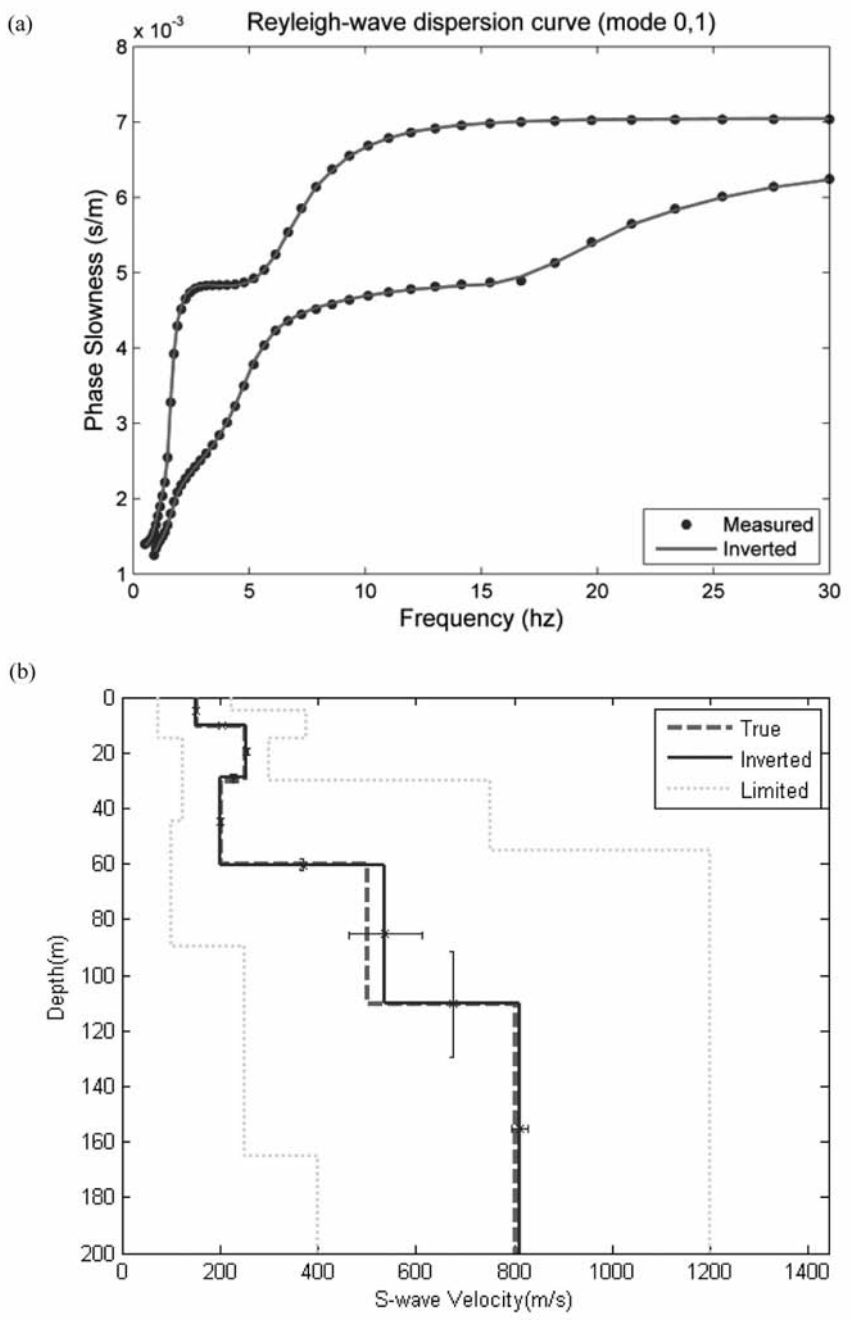

Fig. 14. Inversion of dispersion curve using MPSO for model C. (a) First higher mode (solid dots) and modeled dispersion curve (solid line). (b) The lower and upper bounds (50%) of the search area (dash-dots lines), true model (dashed line) and inverted S-wave velocity profile with standard deviation (solid line).

Comparison between PSO, GA and MPSO

One feature of the MPSO method is the convergence and stability of the models. To further highlight this feature, we again use Model B to implement a Rayleigh-wave dispersion curve inversion scheme by genetic algorithms (GA) developed by Yamanaka and Ishida (1996) and PSO by Eberhart and Shi (2000). We set the population size to 50, crossover probability to 0.7, and mutation probability to 0.03. The algorithm is terminated after 50 iterations. A final solution is determined from an average of 10 trials of random constructions. Fig. 15 summarizes PSO, GA and MPSO inversion results of Rayleigh-wave dispersion curves. As shown here, the misfit values for PSO and GA rapidly decrease in the first 20 iterations, and then gradually converge to a minimum of 10^{-3} in the next 30 iterations. Here the MPSO algorithm has the greatest convergence rate as the misfit is reduced to 10^{-4}. A great deal of the computation time for the models presented here was caused by the forward problems in function evaluations, whereas the inversion scheme used here was fast. By comparison (see Fig. 15) the MPSO outperforms the GA and PSO algorithms in terms of quality of the solutions.

EXPERIMENTAL DATA INVERSION

After testing the applicability of MPSO algorithm in various synthetic models, the MPSO was applied to the dispersion curve derived from microtremor records in a real site. The selected site was located at Golestan Park, Tabriz, north-east of Iran (Fig. 16a). Three non-simultaneous arrays were recorded with radii of 20, 40 and 60 m (Fig. 16b). Due to the near borehole, soil structure mainly consisted of a sequence of sandy-clay, clay, marl and gravel horizontal layers overlying a Miocene marl bedrock (Fig. 17a). Similar to the inverse strategy of the synthetic data, S-wave, P-wave velocities (the assumption of $0.2 <$ Poisson's ratio < 0.5) and thicknesses of layer were considered as variables while fixing densities. Search space and densities adopted for nonlinear inversion of the MPSO approach are reported in Table 5.

Table 5. Real model parameterization to evaluate calculation efficiency and stability of MPSO.

	Layer	Thickness (m) Search Space	V_P (m/s) Search Space	V_S (m/s) Search Space	Density (kg/m^3)
Real Model	1	10-50	400-1200	100-400	1800
	2	10-50	800-2000	300-1000	2000
	3	20-60	1000-3000	500-1200	2000
	4	Half-space	2000-4000	800-2000	2100

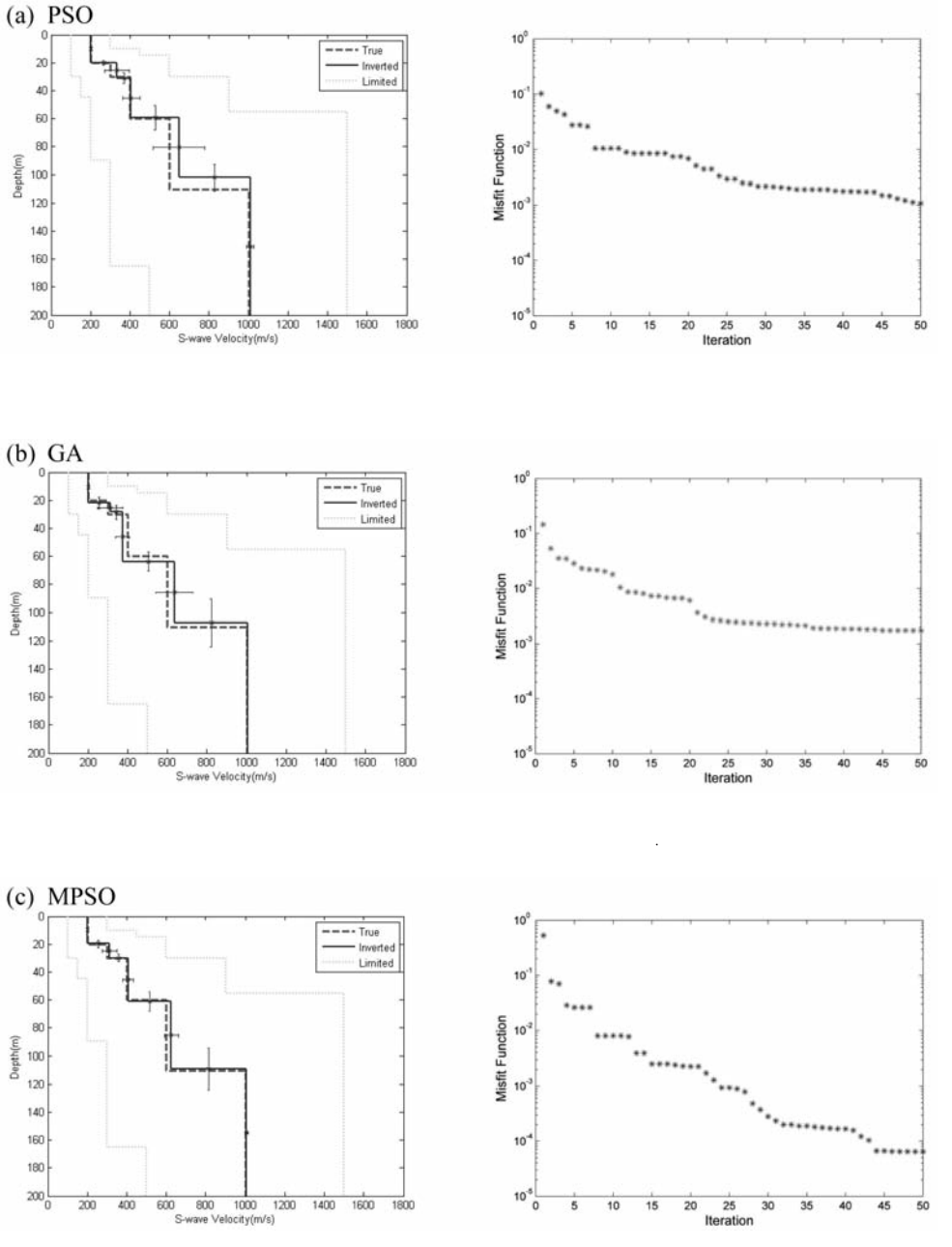

Fig. 15. Comparing the Inversion of dispersion curve using PSO (a), GA (b) and MPSO (c) for model B. (Left column) The lower and upper bounds (50%) of the search area (dash-dots lines), true model (dashed line) and inverted S-wave velocity profile with standard deviation (solid line). (Right column) Misfit behavior of algorithm iteration.

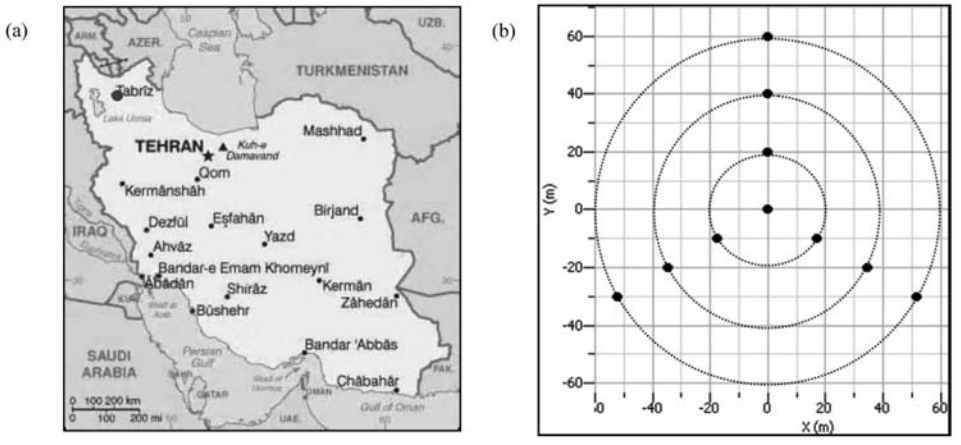

Fig. 16. Location map for the real case at Golestan park, Tabriz, north-east of Iran •, (a) Regional map. (b) Location of all the seismic stations. Three non-simultaneous arrays were recorded: (radii 20, 40 and 60 meter).

During the inversion procedure, a suggested 4-layer subsurface structure was adopted to perform an MPSO inversion of the observed dispersion curve. Inversion results of MPSO for the real example are illustrated in Fig. 17. Panel c in this figure includes a limited frequency spectrum (approximately 2-8 Hz). Panel d here shows the convergence process of MPSO iteration for this example. It is seen here that misfit is significantly decreased in the first 10 iterations and then converged to a similar constant value. This indicates that the algorithm completed the exploration for an optimum solution.

Fig. 17b reports the best solutions of the implementation from MPSO. In particular, the MPSO-estimated profile was in fairly good agreement with borehole stratigraphy shown in Fig. 17a. The seismic bedrock shear-wave velocity, which consists of marl, sand and gravel, marley sand and gravel, determined from the microtremor, is about 950 m/s. However, the shear-wave velocity determined for the Miocene marl bedrocks is higher than 1400 m/s. Depths of the velocity discontinuities between all layers, including three contrasts (sandy-gravel to clay, clay to sandy-marl and bedrock contacts) were well delineated by MPSO. According to the log stratigraphy, the actual bedrock was found to be 85 meters. We estimated the depth to bedrock to be 81 meters using Rayleigh-wave dispersion curve inversion.

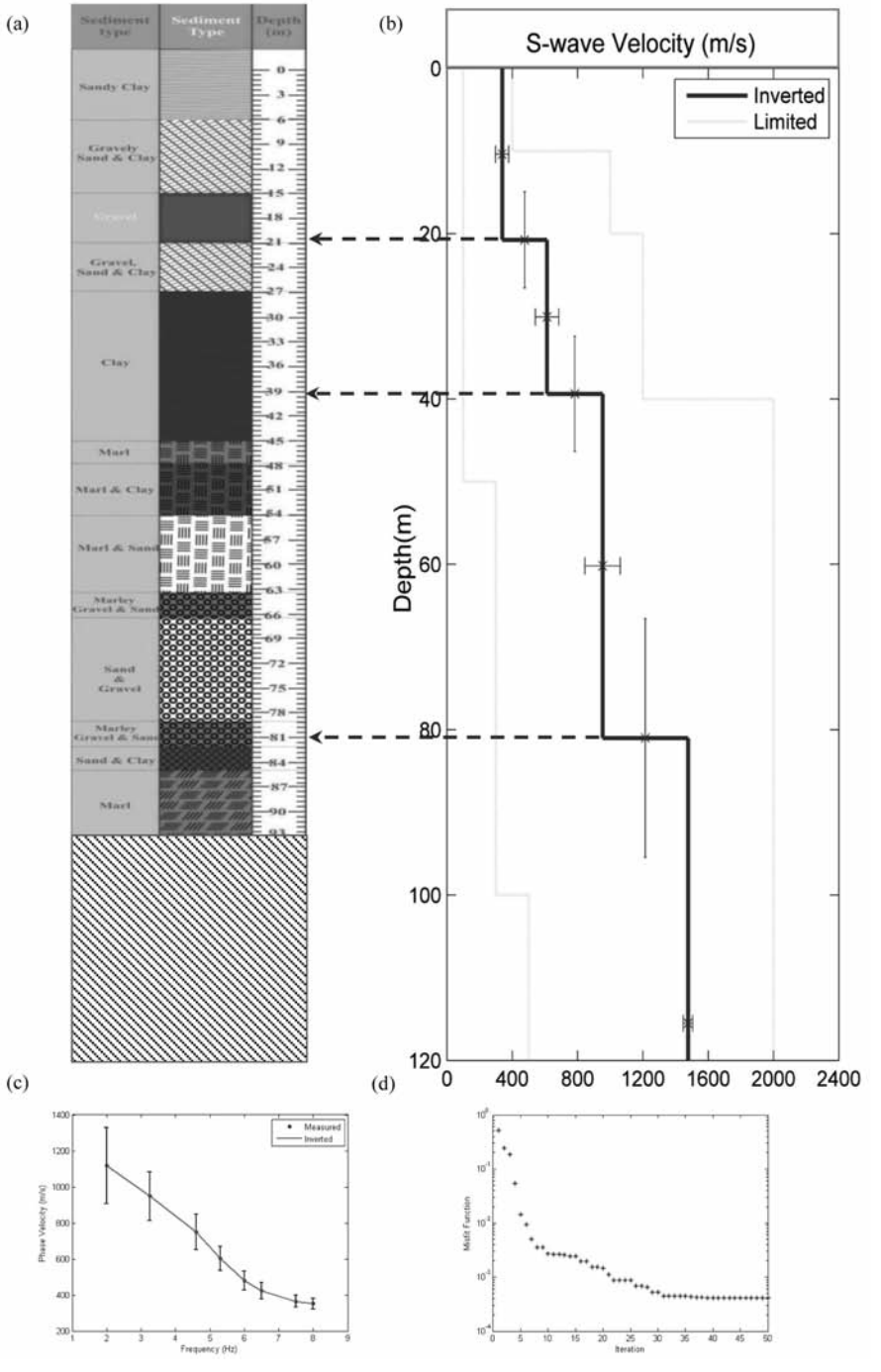

Fig. 17. Inversion of real case data: (a) Borehole description. (b) The lower and upper bounds of the search area (dash-dots lines), inverted and S-wave velocity profile with standard deviation (solid line). (c) Real data (solid dots) and modeled dispersion curve (solid line) Inversion of dispersion curve using MPSO. (d) Misfit behavior of MPSO iteration.

CONCLUSION

A new computer code based on the MPSO algorithm was developed for the inversion of Rayleigh dispersion curves, with the aim of integrating any data resulting from processing of active-source experiments or ambient-noise recordings. Performance of the mutation based particle swarm optimization (MPSO) was investigated for Rayleigh-wave inversion of broadband noise-free, wide search space and noise-added dispersion curve data. Wider search space boundaries were adopted to simulate more realistic cases where a priori information was not available, and also to examine the capability of MPSO approach. According to the present analyses, MPSO was a simple, effective and robust algorithm for inverting Rayleigh-waves. Adding 10% Guassian noise to dispersion curve data from two-layer model had a slight effect on the inversion result; but, adding 10% Guassian noise to dispersion curve data from five-layer models had a considerable effect on the inversion result of the fourth layer. The implementation was tested on four synthetic and one field data sets. The inversions on one field data set yielded S-wave velocity profiles that followed the geological log in a proper manner.

As the main advantages of MPSO, it was found to be easy to implement. Also there were few parameters for adjusting. For the future studies we will be introducing joint inversion of surface waves, in higher mode Rayleigh-waves and Love-waves, for other geophysical data such as refractions and geoelectrics.

ACKNOWLEDGEMENTS

We thank the Research Centre of the Tabriz Metropolis Council for providing the real data experiments of this study. We would like to acknowledge the GEOPSY Software and Service for processing our real data. Also, we would like to thank two anonymous reviewers for the useful and constructive comments which helped improve the content of this paper.

REFERENCES

Aki, K., 1957. Space and time spectra of stationary stochastic waves, with special reference to microtremors. Bull. Earthq. Res. Inst., 35: 415-456.

Angeline, P.J., 1998. Using selection to improve particle swarm optimization. Proc. 1998 Internat. Conf. Evolution. Computat. IEEE Press: 84-89.

Bard, P.Y. and Riepl, J., 1999. Wave propagation in complex geological structures and local effects on strong ground motion. In: Wave Motion in Earthquake Engineering. WIT Press, New York: 38-95.

Beaty, K.S., Schmitt, D.R. and Sacchi, M., 2002. Simulated annealing inversion of multimode Rayleigh wave dispersion curves for geological structure. Geophys. J. Internat., 151: 622-631.

Boore, D., 2006. Determining subsurface shear-wave velocities: a review. 3rd Internat. Symp. Effects of Surface Geology on Seismic Motion, Grenoble: 103.

Capon, J., 1969. High-resolution frequency-wavenumber spectrum analysis. Proc. IEEE, 57: 1408-1418.

Cercato, M., 2009. Addressing non-uniqueness in linearized multichannel surface wave inversion. Geophys. Prosp., 57: 27-47.

Clerc, M., 1999. The swarm and the queen: Towards a deterministic and adaptive particle swarm optimization. Proc. 1999 Congr. Evolution. Computat. IEEE Press, New York: 1951-1957.

Clerc, M. and Kennedy, J., 2002. The particle swarm-explosion, stability, and convergence in a multidimensional complex space. IEEE Transact. Evolution. Computat., 6: 58-73.

Dal Moro, G., Pipan, G. and Gabrielli, M.P., 2007. Rayleigh wave dispersion curve inversion via genetic algorithms and marginal posterior probability density estimation. J. Appl. Geophys., 61: 39-55.

Dal Moro, G. and Ferigo, F., 2011. Joint analysis of Rayleigh and Love wave dispersion for near-Surface studies: issues, criteria and improvements. J. Appl. Geophys., 75: 573-589.

Dasios, A., McCann, C., Astin, T., McCann, D. and Fenning, P., 1999. Seismic imaging of the shallow subsurface: shear wave case histories. Geophys. Prosp., 47: 565-591. doi: 10.1046/j.1365-2478.1999.00138.x.

Dumitrescu, D., Lazzerini, B., Jain, L.C. and Dumitrescu, A., 2000. Evolutionary Computation. CRC Press, New York.

Dunkin, J.W., 1965. Computation of modal solutions in layered, elastic media at high frequencies. Bull. Seismol. Soc. Am., 55: 335-358.

Eberhart, R.C. and Shi, Y., 2000. Comparing inertia weights and constriction factors in particle swarm optimization. Proc. 2000 Congr. Evolution. Computat., IEEE Press: 84-88.

Eberhart R., and Kennedy J. 1995. A new optimizer using particle swarm theory, Proceedings of the Sixth International Symposium on Micro Machine and Human Science. IEEE Press, p. 39-43.

Esmin, A.A.A., Lambert-Torres, G. and Zambroni, A.C., 2005. A hybrid particle swarm optimization applied to loss power minimization. IEEE Trans. Power Syst., 20: 859-866.

Esmin, A.A.A., Lambert-Torres, G. and Alvarenga, G.B., 2006. Hybrid evolutionary algorithm based on PSO and GA mutation. Proc. 6th Internat. Conf. Hybrid Intell. Syst.: 57-57.

Foti, S., Comina, C., Boiero, D. and Socco, L.V., 2009. Non-uniqueness in surface wave inversion and consequences on seismic site response analyses. Soil Dynam. Earthq. Engin., 29: 982-993.

Gao, H. and Wenbo, X.W., 2011. Particle swarm algorithm with hybrid mutation strategy. Appl. Soft Comput., 11: 5129-5142.

Goldberg, D.E., 1989. Genetic Algorithms in search, optimization, and machine learning. Addison-Wesley Publishing Corporation, Inc., New York.

Haskell, N.A., 1953. The dispersion of surface waves on a multi-layered medium. Bull. Seismol. Soc. Am., 43: 17-34.

Hunter, J., Benjumea, B., Harris, J., Miller, R., Pullan, S. and Burns, R.A., 2002. Surface and down hole shear wave seismic methods for thick soil site investigations. Soil Dynam. Earthq. Engin., 22: 931-941. doi: 10.1016/S0267-7261-02-00117-3.

Jongmans, D., 1992. The application of seismic methods for dynamic characterization of soils in earthquake engineering. Engin. Geol., 46: 63-69. doi: 10.1007/BF02595035.

Kennedy, J. and Eberhart, R.C., 1995. Particle swarm optimization. Proc. IEEE Int. Conf. Neural Netw., 4: 1942-1948.

Kennedy, J. and Eberhart, R.C., 2001. Swarm intelligence. Morgan Kaufmann Publishers, Inc., San Francisco.

Knopoff, L., 1964. Amatrix method for elastic wave problems. Bull. Seismol. Soc. Am., 54: 431-438.

Kvaerna, T. and Ringdahl, F., 1986. Stability of various fk-estimation techniques. Semiann. Techn. Summ., 1 Oct. 1985 - 31 March 1986, NORSAR Scient. Rep., 1-86/87, Kjeller, Norway: 29-40.

Lacoss, R.T., Kelly, E.J. and Toksöz, M.N., 1969. Estimation of seismic noise structure using arrays. Geophysics, 34: 21-38.

Lu, H., Sriyanyong, P., Song, Y.H. and Dillon, T., 2010. Experimental study of a new hybrid PSO with mutation for economic dispatch with non-smooth cost function. Electr. Power Energy Syst., 32: 921-935.

Luo, Y., Xia, J., Miller, R.D., Xu, Y., Liu, J. and Liu, Q., 2009. Rayleigh-wave mode separation by high-resolution linear Radon transform. Geophys. J. Internat., 179: 254-264.

Maraschini, M. and Foti, S. 2010. A Monte Carlo multimodal inversion of surface waves. Geophys. J. Internat., 182: 1557-1566.

McMechan, G.A. and Yedlin, M.J., 1981. Analysis of dispersive waves by wave field transformation. Geophysics, 46: 869-874.

Metropolis, N., Rosenbluth, M.N., Rosenbluth, A.W., Teller, A.H. and Teller, E., 1953. Equation of state calculations by fast computing machines. J. Chem. Phys., 21: 1087-1092.

Ohrnberger, M. 2001. Continuous automatic classification of seismic signals of volcanic origin at Mt. Merapi, Java, Indonesia. Ph.D. thesis, Univ. of Potsdam.

Pan, Y., Xia, J., Gao, L., Shen, C. and Zeng, C. 2013. Calculation of Rayleigh-wave phase velocities due to models with a high-velocity surface layer. J. Appl. Geophys., 96: 1-6.

Park, C.B., Miller, R.D. and Xia, J., 1998. Imaging dispersion curves of surface waves on multi-channel record, Technical Program with Biographies. Expanded Abstr., 68th Ann. Internat. Mtg., New Orleans: 1377-1380.

Pei, D., Louie, J.N. and Pullammanappallil, S.K., 2007. Application of simulated annealing inversion on high-frequency fundamental-mode Rayleigh wave dispersion curves. Geophysics, 72: R77-R85.

Pezeshk, S. and Zarrabi, M., 2005. A new inversion procedure for spectral analysis of surface waves using a genetic algorithm. Bull. Seismol. Soc. Am., 95: 1801-1808.

Press, W.H., Teukolsky, S.A., Vetterling, W.T. and Flannery, B.P., 1992. Numerical Recipes in Fortran, 2nd ed. Cambridge University Press, Cambridge.

Ratnaweera, A., Halgamuge, S.K. and Watson, H.C., 2004. Self-organizing hierarchical particle swarm optimizer with time-varying acceleration coefficients. IEEE Transact. Evolution. Comput., 8: 240-255.

Renalear, F., Jongmans, D., Savvaidis, A., Wathelet, M., Endrun, B. and Cornou, C. 2010. Influence of parameterization on inversion of surface wave dispersion curves and definition of an inversion strategy for sites with a strong V_S contrast. Geophysics, 75(6): 197-209.

Roberts, J.C. and Asten, M.W. 2004. Resolving a velocity inversion at the geotechnical scale using the microtremor (passive seismic) survey method. Explor. Geophys., 35: 14-18.

Sambridge, M., 1999. Geophysical inversion with a neighbourhood algorithm-I. Searching parameter space. Geophys. J. Internat., 138: 479-494.

Satoh, T., Kawase, H. and Matsushima, S.I., 2001. Differences between site characteristics obtained from microtremors, S-waves, P-waves, and codas. Bull. Seismol. Soc. Am., 91: 313-334.

Sen, M.K. and Stoffa, P.L., 1996. Bayesian inference, Gibb's sampler and uncertainty estimation in geophysical inversion. Geophys. Prosp., 44: 313-350.

Shi, Y. and Eberhart, R., 1998. A modified particle swarm optimizer. Proc. 1998 Internat. Conf. Evolution. Computat. IEEE Press: 69-73.

Socco, L.V. and Jongmans, D. 2004. Special issue on seismic surface waves. Near Surface Geophys., 2: 163-165.

Socco, L.V. and Boiero, D. 2008. Improved Monte Carlo inversion of surface wave data. Geophys. Prosp., 56: 357-371.

Socco, L.V., Foti, S. and Boiero, D., 2010. Surface-wave analysis for building near-surface velocity models - Established approaches and new perspectives. Geophysics, 75(4): 83-102.

Somerville, P.G. and Graves, R.W., 2003. Characterization of earthquake strong ground motion. Pure Appl. Geophys., 160: 1811-1828. doi: 10.1007/s00024-003-2407-z.

Stoffa, P.L. and Sen, M.K., 1992. Seismic waveform inversion using global optimization. J. Seismic Explor., 1: 9-27.

Thomson, W.T., 1950. Transmission of elastic waves through a stratified solid medium. J. Appl. Phys., 21: 89-93.

Triki, E., Collette, Y. and Siarry, P., 2005. A theoretical study on the behavior of simulated annealing leading to a new cooling schedule. Europ. J. Operat. Res., 166: 77-92.

Wathelet, M., Jongmans, D. and Ohrnberger, M., 2004. Surface wave inversion using a direct search algorithm and its application to ambient vibration measurements. Near Surface Geophys., 2: 211-221.

Xia, J., Miller, R.D. and Park, C.B., 1999. Estimation of near-surface shear-wave velocity by inversion of Rayleigh wave. Geophysics, 64: 691-700.

Xia, J., Miller, R.D., Park, C.B. and Tian, G., 2003. Inversion of high-frequency surface waves with fundamental and higher modes. J. Appl. Geophys., 52: 45-57.

Xia, J., Xu, Y. and Miller, R.D., 2007. Generating image of dispersive energy by frequency decomposition and slant stacking. Pure Appl. Geophys., 164: 941-956.

Yamanaka, H. and Ishida, H. 1996. Application of genetic algorithms to an inversion of surface-wave dispersion data. Bull. Seismol. Soc. Am., 86: 436-444.

Yilmaz, Í., 1987. Seismic Data Processing. SEG, Tulsa, OK.